

A Kinetic Study on the Evolution of Martensitic Transformation Behavior and Microstructures in Ti–Ta High-Temperature Shape-Memory Alloys During Aging

Alexander Paulsen¹ · Jan Frenzel¹ · Dennis Langenkämper¹ · Ramona Rynko¹ · Peter Kadletz^{2,3} · Lukas Grossmann² · Wolfgang W. Schmahl² · Christoph Somsen¹ · Gunther Eggeler¹

Published online: 18 December 2018
© ASM International 2018

Abstract Ti–Ta alloys represent candidate materials for high-temperature shape-memory alloys (HTSMAs). They outperform several other types of HTSMAs in terms of cost, ductility, and cold workability. However, Ti–Ta alloys are characterized by a relatively fast microstructural degradation during exposure to elevated temperatures, which gives rise to functional fatigue. In the present study, we investigate how isothermal aging affects the martensitic transformation behavior and microstructures in Ti₇₀Ta₃₀ HTSMAs. Ti–Ta sheets with fully recrystallized grain structures were obtained from a processing route involving arc melting, heat treatments, and rolling. The final Ti–Ta sheets were subjected to an extensive aging heat treatment program. Differential scanning calorimetry and various microstructural characterization techniques such as scanning electron microscopy, transmission electron microscopy, conventional X-ray, and synchrotron diffraction were used for the characterization of resulting material states. We identify different types of microstructural

evolution processes and their effects on the martensitic and reverse transformation. Based on these results, an isothermal time temperature transformation (TTT) diagram for Ti₇₀Ta₃₀ was established. This TTT plot rationalizes the dominating microstructural evolution processes and related kinetics. In the present work, we also discuss possible options to slow down microstructural and functional degradation in Ti–Ta HTSMAs.

Keywords High-temperature shape-memory alloys · Martensitic transformation · Microstructure · Phase stability · Precipitation · Omega phase

Introduction

Shape-memory alloys (SMAs) represent functional materials, which are able to re-establish their initial geometry after deformations significantly exceeding typical elastic strains [1–4]. Two different types of shape-memory effects, a thermal (one/two way effect) and a mechanical memory (pseudoelasticity) are used in applications [5–8]. Both effects rely on a reversible martensitic phase transformation [1–4, 9]. The low-temperature phase martensite forms during cooling between the martensite start and finish temperatures, M_S and M_F , or during mechanical loading when reaching a critical stress level σ_{AM} . The reverse transformation can be observed during heating between the austenite start and finish temperatures, A_S and A_F , and during unloading to σ_{MA} .

The thermal shape-memory effect is often exploited in actuators which are integrated in technological systems [5, 10]. For actuation, SMAs are thermally activated to provide a mechanical work output. A deformation applied at low temperatures, where the material shows a twinned

This article is an invited paper selected from presentations at the 2nd International Conference on High-Temperature Shape-Memory Alloys and has been expanded from the original presentation. HTSMA 2018 was held in Irsee, Germany, May 15–18, 2018, and was organized by the German Materials Society (DGM).

✉ Alexander Paulsen
alexander.paulsen@rub.de

- ¹ Institute for Materials, Ruhr University Bochum, Universitätsstraße 150, 44801 Bochum, Germany
- ² Applied Crystallography and Materials Science, Department of Earth and Environmental Sciences, Faculty of Geosciences, Ludwig-Maximilians-Universität, 80333 Munich, Germany
- ³ European Spallation Source ESS ERIC, P.O. Box 176, 22100 Lund, Sweden

martensitic microstructure, causes the growth of preferentially oriented variants [1–4]. On heating, the material transforms back to austenite. This reverse transformation re-establishes the initial geometry because austenite does *not* form variants. During subsequent cooling to ambient temperature, the material again transforms to martensite.

Progress in shape-memory technology demands SMAs which are characterized by high transformation temperatures [11–15]. These materials need to show a reversible martensitic transformation in a temperature range which is significantly higher as compared to binary Ni–Ti, the most commercially successful SMA at present. Technological systems often operate at elevated temperatures, and uncontrolled self-actuation must be avoided [11–15]. Various HTSMA systems are being considered as potential candidate materials, e.g., Ni–Ti–Au [16], Ni–Ti–Pd [17, 18], Ni–Ti–Pt [19], Ni–Ti–Zr [20, 21], Ni–Ti–Hf [20–22], and others [23–28]. While a good progress could be achieved during the last decades, still severe drawbacks/difficulties remain unsolved or still challenging. For example, Ni–Ti–Au, Ni–Ti–Pd, Ni–Ti–Pt are expensive due to their high contents of noble metals. Ni–Ti–Zr and Ni–Ti–Hf are relatively brittle (especially in the as cast state) [11, 22, 29–31]. For this reason, it is difficult (but also not impossible [30]) to prepare semi-parts such as thin wires or sheets, which are often required for the design of shape-memory actuators.

Ti–Ta-based alloy compositions have received increasing scientific attention as they combine specific properties which make them attractive as HTSMAs. They do not contain expensive noble metals, and they exhibit excellent ductility and cold workability [32, 33]. Ti–Ta SMAs can be classified as β titanium alloys [28, 34, 35]. Figure 1 shows the phase diagram of the binary system Ti–Ta [36]. Pure Ti shows an allotropic transformation of type β (bcc) \leftrightarrow α

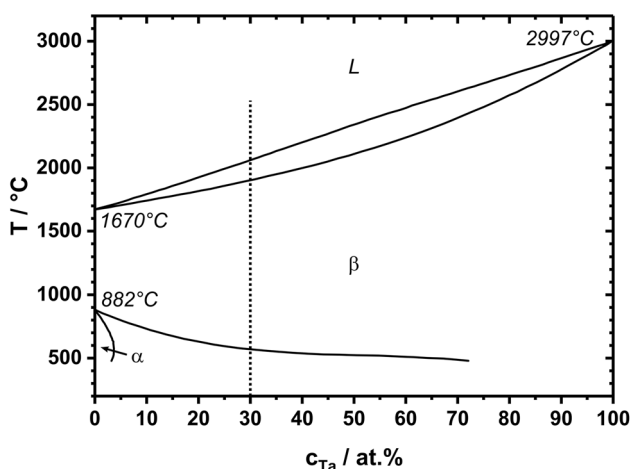


Fig. 1 Suggested phase diagram of the binary system Ti–Ta [36]. The dashed line represents the composition of a Ti₇₀Ta₃₀ HTSMA

(hex) phase at 882 °C. In Ti alloys, the β phase represents the high-temperature austenite phase. The addition of Ta allows to stabilize the β phase by decreasing the $\beta \leftrightarrow (\alpha + \beta)$ transformation temperature. Furthermore, the β phase can be stabilized at lower temperatures by solution annealing and subsequent quenching. In this metastable state, the HTSMA shows a martensitic transformation of type $\beta \rightarrow \alpha''$, which can provide a shape-memory effect. To our knowledge, the formation of α'' martensite in Ti–Ta was reported for the first time by Bagarjatskii et al. in 1958 [37]. An evidence for the shape-memory effect in the Ti–Ta system was reported for the first time by Petrzhik et al. [38]. The research group of Miyazaki later investigated aspects related to alloy compositions and mechanical/functional behavior [32, 39–41]. Recently, fundamental effects of compositions on phase stabilities [42–44], processing [33], creep [45], functional and structural fatigue [46–49], aspects related to biocompatibility [50, 51], and the preparation of Ti–Ta thin films [52, 53] have been investigated. In recent publications [43, 44], the effects of Ta and Al concentrations on M_s were investigated with focus on the generation of precise reference data sets and on the identification of underlying mechanisms.

Unfortunately, Ti–Ta alloys do not match all criteria which are desired for a “general purpose” HTSMA. The most severe drawback as compared to other HTSMA systems is a relatively poor functional/structural stability [40, 46–49]. The exposure of Ti–Ta to elevated temperatures, e.g., 250 °C < T < 600 °C, is associated with precipitation processes which significantly affect the martensitic transformation and thus shape-memory behavior. It has been recently shown that the corresponding microstructural changes govern functional fatigue in Ti–Ta HTSMA actuators during functional cycling [46–49]. The dashed vertical line in the phase diagram, Fig. 1 [36], represents a Ti₇₀Ta₃₀ HTSMA, a common composition considered in earlier studies, e.g., [33, 40, 46]. As shown in Fig. 1, a Ti₇₀Ta₃₀ HTSMA is characterized by the presence of β phase as a single phase at temperatures between 580 and 1900 °C. However, from the Ti–Ta phase diagram [36], Fig. 1, one can conclude that the exposure to temperatures below 580 °C results in thermodynamic driving forces which act to establish an equilibrium state consisting of two phases, Ti-rich α and Ta-rich β . Furthermore, these two phases are not the only phases which can form in this material. Similar to other β stabilized Ti alloys, e.g., [54–56], Ti–Ta is known for the formation of ω phase (not included in the phase diagram, Fig. 1) [40, 41, 49]. In general, ω phase (hexagonal) can form in Ti alloys during isothermal annealing, rapid cooling, and mechanical deformation [57, 58] by a collapse of the $\{111\}_\beta$ planes [40, 41, 49]. Precipitation of ω phase is known to affect

mechanical properties and also the formation of α'' martensite [54–56]. The ω phase in Ti (and also in other alloys) is often considered as a metastable phase, e.g., [59, 60], which acts as a precursor for the α phase at intermediate aging temperatures. However, its metastable nature is not always evident. It is documented in literature that the ω phase still could be observed in some Ti alloys after relatively long isothermal aging heat treatments, e.g., [61, 62].

The objective of the present study is to provide an overview on the evolution of martensitic transformation behavior and microstructures during isothermal aging of $\text{Ti}_{70}\text{Ta}_{30}$ HTSMAs. We investigate how specific features of the martensitic and reverse transformation are affected by the formation of different types of microstructures. We combine advanced thermal and microstructural characterization methods to investigate different material states resulting from extensive isothermal aging experiments. Maximum aging durations close to 1 month were considered. The present work contributes to a better understanding of functional, thermodynamic, and kinetic aspects of Ti–Ta-based HTSMAs.

Experiments

Materials, Processing, and Aging Heat Treatments

In the present study, we consider a $\text{Ti}_{70}\text{Ta}_{30}$ HTSMA. A series of 10 ingots with masses close to 50 g was prepared by arc melting using high-purity Ti (99.995 wt%) and Ta (99.95 wt%) raw materials, obtained from Hauner Metallische Werkstoffe (Röttenbach, Germany). A melter of type Edmund Bühler AM was used for alloy preparation. The Ti–Ta ingots were remelted 12 times, and they were held at least for 20 s in the liquid state, to ensure sufficient mixing of Ti and Ta. All details on the melting process are given elsewhere [33, 63]. After solidification, the ingots were homogenized at 1100 °C for 25 h under vacuum in order to minimize microscale heterogeneities associated with dendritic solidification [33]. All resulting samples were subjected to thermomechanical processing involving cold rolling and intermediate heat treatments at 900 °C for 10 min followed by water quenching. All details on processing are available in literature [33]. The final material state, fully recrystallized sheets with a thickness of 1 mm

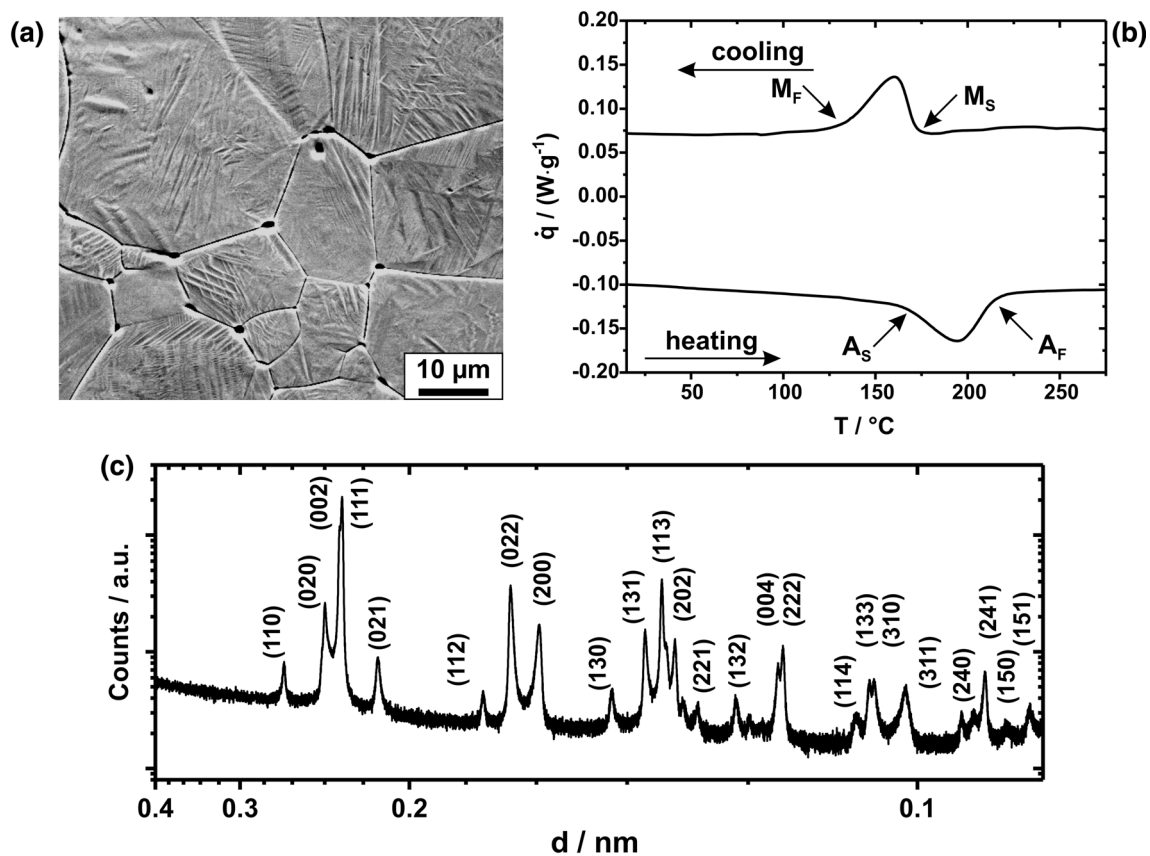


Fig. 2 Microstructural details and phase transformation behavior of the initial material state used for aging experiments. **a** SEM micrograph showing α'' martensite and prior β grain boundaries. We note that the dark/bright fringes in grain boundary regions are

related to etching. They do not represent another phase. **b** DSC chart, **c** XRD data documenting the presence of α'' martensite as the only microstructural constituent

were obtained after applying a degree of deformation of $\varphi = 0.9$ followed by recrystallization annealing at 900 °C for 10 min in argon atmosphere and water quenching.

The microstructures and phase transformation characteristics of all ten sheets resulting from the ten ingots were carefully evaluated in order to exclude differences in material behavior. Figure 2 exemplarily provides microstructural details from one $\text{Ti}_{70}\text{Ta}_{30}$ sheet which is representative for the initial material state used for aging experiments. The SEM micrograph in Fig. 2a shows that this HTSMA sheet is characterized by an equiaxed grain structure with an average grain size close to 20 μm . At room temperature, the alloy is in the martensitic state, as can be seen from the high density of martensite twins. We note that α'' is the only phase in this material state. The dark/bright fringes in grain boundary regions in Fig. 2a are related to etching. The DSC chart in Fig. 2b shows the transformation behavior of this material state. The exothermic peak on cooling is related to the martensitic transformation, and the endothermic peak on heating to the reverse transformation. The martensite start temperature M_S is close to 180 °C, which is in line with literature data for $\text{Ti}_{70}\text{Ta}_{30}$ [41, 43, 44]. Figure 2c presents a conventional X-ray diffractogram which suggests that α'' martensite represents the only phase in this material at room temperature (no other peaks could be detected). Martensite lattice parameters $a = 0.31968$ nm, $b = 0.47854$ nm, and $c = 0.46347$ nm could be derived from the data shown in Fig. 2c.

Aging Heat Treatments

Rectangular samples which had been previously cut from the Ti–Ta HTSMA sheets were used for aging experiments. The resulting material states were investigated by differential scanning calorimetry (DSC), scanning electron microscopy (SEM), transmission electron microscopy (TEM), conventional X-ray diffraction (XRD), and synchrotron X-ray diffraction (SD). Figure 3 specifies aging temperatures and aging durations, as well as the different characterization techniques which were applied for the investigation of the different material states. In the present study, a temperature window ranging from 250 to 800 °C with aging durations up to 41,616 min (≈ 29 days) was considered. Figure 3 documents that a large number of different material states was systematically evaluated.

Prior to aging experiments, samples with sizes close to 20 mm \times 12 mm \times 1 mm were extracted from the Ti–Ta HTSMA sheets by a low-speed metallographic saw of type Lenco VC-50. All sample surfaces were polished using 180 mesh SiC paper in order to remove oxide layers. After subsequent ultrasonic cleaning, the samples were subjected to aging heat treatments. Two different types of heat

treatment systems were used in the present study. First, a convection furnace of type Heraeus K750/1 was used for aging experiments with short durations between 1 and 25 min in a temperature range of 250–400 °C. This furnace allowed to quickly heat the samples to the desired temperature by fan-forced circulating air. Second, a vacuum/protective atmosphere tube furnace of type Carbolite HVT 12/80/700/E301 was used for all other aging experiments. During heating to the target temperature, the furnace was continuously evacuated to maintain a constant pressure of approximately 3×10^{-5} mbar. The system was filled with high-purity argon (99.9999 vol%), right before the Ti–Ta samples were inserted into the heated zone. The different Ti–Ta HTSMA samples were previously mounted in a special holder, where they had been shielded with Ti-sheets in order to keep oxidation at a minimum. Aging experiments were conducted at a slight overpressure of 20 mbar and a flow rate of argon close to 0.2 l/min. After aging, the samples were quickly removed from the hot furnace and quenched in water in order to freeze the microstructures resulting from the heat treatment. We note that the samples could be removed from the furnace and quenched within less than 2 s.

Thermal Analysis, Microstructural, and Chemical Characterization

The phase transition behavior of different material states was evaluated using DSC. Specimens with masses of ≈ 50 mg were investigated in an instrument of type TA 2920 CE. The heating and cooling rate was 20 K/min. Initially, the samples were heated up to the maximum test temperature ($T_{\text{max}} = 300$ °C), held for 2 min followed by

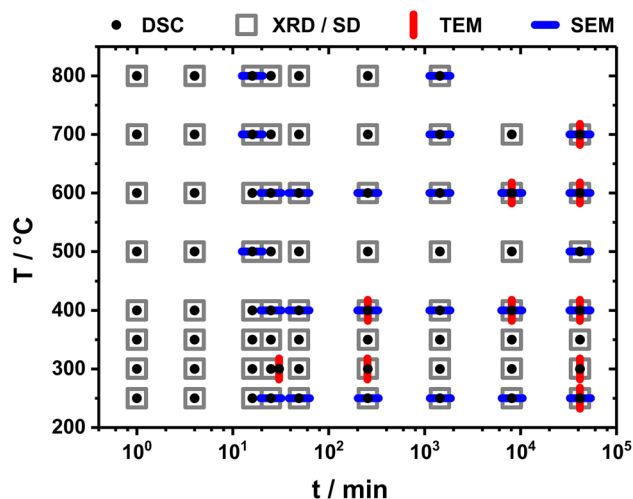


Fig. 3 Experimental frame for aging experiments. Specification of aging temperatures, aging durations, and applied characterization techniques (Color figure online)

subsequent cooling to 20 °C. The start and finish temperatures of the martensitic transformation (M_S and M_F) and of the reverse transformation (A_S and A_F) were determined using the tangent method. Details on DSC sample preparation are given in Refs. [33, 63].

For the characterization of microstructures, an SEM of type FEI ESEM Quanta FEG 650 SEM was used. This SEM is equipped with an energy dispersive X-ray (EDX) analyzer of type EDAX Apollo XPP. Microchemical analysis was applied to assess chemical compositions of various microstructural constituents in aged material states. Samples for SEM characterization were prepared by common metallography procedures. Final metallographic sample states were obtained after vibro polishing using an instrument of Buehler VibroMet. A colloidal silica suspension with an average particle size of 0.25 μm containing H_2O_2 was used. Secondary electron (SE) contrast allowed to visualize martensitic microstructures, whereas back scatter electrons (BSE) provided chemical contrast. For the visualization of martensite by SE contrast, one sample was additionally etched using a solution of 100 ml water and 5 g ammonium hydrogen difluoride. The TEM investigations were performed on a FEI Tecnai F20 G² Supertwin, operated at a nominal acceleration voltage of 200 kV. The system is equipped with a high-angle annular area dark-field (HAADF) detector, with scanning unit, and with an EDX system from EDAX. For TEM sample preparation, a focused ion beam (FIB) system of type FEI Quanta 200 3D Dual Beam SEM was used.

A diffractometer of type Philips X'Pert PW3050/65, equipped with a copper tube, a hybrid monochromator with a 1/4° aperture providing Cu-K_{α1} radiation, and a X'Celerator line detector were used for crystallographic analysis. The scanning rate was 0.002842°/s, and the increment between two steps was 0.006°. Le Bail refinement implemented in the software MAUD [64, 65] was used to interpret diffraction data and to identify phases. In addition to conventional XRD, synchrotron diffraction was performed at the DESY PETRA III high-resolution powder diffraction beamline P02.1 in Hamburg, Germany. The experiments were characterized by a beam wavelength of 0.0207 nm, and a beam cross section of 1 × 1 mm². A detector of type PerkinElmer XRD1621 was used to acquire diffraction data. The distance between the Ti-Ta sample and the detector was 853 mm. SD powder diffractograms were also evaluated using the software MAUD [64, 65]. Further details on the beamline setup are available in literature [66]. We note that XRD and SD analyses were carried out at room temperature on quenched material states.

The chemical purity of different material states was characterized in terms of oxygen using inert gas fusion IR method. Chemical analyses were subcontracted to

Revierlabor (Essen, Germany). The oxygen concentration of the initial material state used for aging experiments was close to 0.04 wt%. A slight increase could be observed in case of long-term aging at high temperatures. Only one sample exceeded 0.1 wt% O (700 °C/41,616 min), and it was therefore excluded from thermal analysis.

Results

Influence of Aging on Phase Transformation Behavior

In the present study, the microstructural and functional stability of Ti₇₀Ta₃₀ HTSMAs has been evaluated in a time/temperature window specified in Fig. 3. Figure 4 provides results on the influence of aging heat treatments on the martensitic and reverse phase transformation. DSC charts obtained from three different aging temperatures, 250 °C (Fig. 4a and b), 400 °C (Fig. 4c and d), and 600 °C (Fig. 4e and f) are exemplarily presented. The left column of Fig. 4 compiles DSC data obtained during cooling from the high-temperature phase. The exothermic peaks indicate the formation of martensite. The right column of Fig. 4 shows data obtained during heating from the low-temperature regime. The endothermic peaks are associated with the transformation from α' martensite to the high-temperature β phase. The color code in the legend (upper part of Fig. 4) specifies the different aging durations. Our DSC results show that, generally, the transformation behavior of Ti₇₀Ta₃₀ HTSMAs is significantly affected by isothermal aging. In case of aging at a low temperature of 250 °C, Fig. 4a and b, the following trends can be identified. With increasing aging time, (1) the temperature where martensite forms decreases, and (2) the latent heat, i.e., the area below the transformation peak, becomes smaller, Fig. 4a. A similar behavior has been observed for the reverse transformation on heating, whereas a slight increase of the austenite peak temperature occurred in the earlier aging stages, Fig. 4b. After 256 min aging, no transformation processes could be detected by DSC, as indicated by flat heat flow curves. This finding suggests that the corresponding material states do not show a shape-memory effect.

In case of aging at a higher temperature of 400 °C, Fig. 4c and d, no martensitic transformation can be detected after 16 min thermal exposure. However, the DSC data obtained during heating of this material state still reveal weak transformation events associated with the formation of austenite. The related DSC peaks slightly shift to higher temperatures with increasing heat treatment duration. Finally, after 256 min aging, the situation changes and no transformation events can be detected, Fig. 4d.

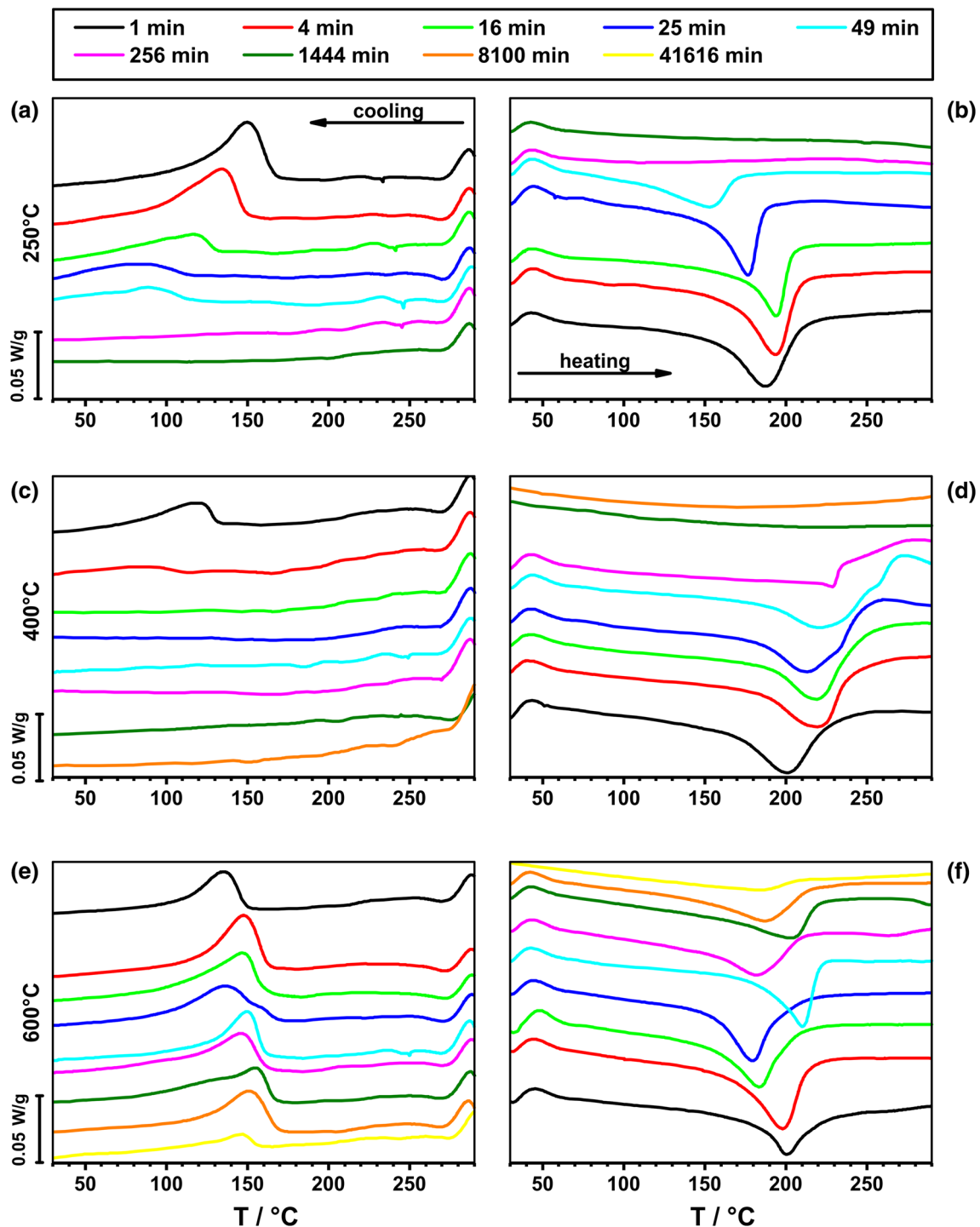


Fig. 4 DSC data obtained from $\text{Ti}_{70}\text{Ta}_{30}$ after different aging treatments conducted at (a and b) 250 °C, (c and d) at 400 °C, and (e and f) at 600 °C. The left column (a, c, and e) shows heat flow data obtained during cooling from high temperature. We note that only the large spikes

are related to transformation events. The small peaks occasionally obtained at temperatures close to 240 °C represent small DSC artifacts. The right column (b, d, and f) provides heat flow data related to heating from the low-temperature regime (Color figure online)

The results obtained from aging at a higher temperature of 600 °C, Fig. 4e and f, differ from what has been previously shown. In this case, aging results in relatively slight changes in phase transformation temperatures, and all

material states—even after a long thermal exposure for ≈ 29 days (41,616 min)—exhibit defined phase transformation processes on cooling and heating. However, the latent heats associated with the martensitic and reverse

transformation are lower for the case of long aging durations (compare yellow and black lines in Fig. 4e and f).

Figure 5 presents a compilation of data which show how aging temperatures and aging durations affect M_S in $\text{Ti}_{70}\text{Ta}_{30}$ HTSMAs. The data points in Fig. 5 were derived from DSC charts as previously shown in Fig. 4. In case of aging in a relatively low temperature range, such as from 250 °C to 400 °C, Fig. 5a, the associated microstructural changes result in a rapid decrease of M_S . The strongest change was observed for annealing at 400 °C where a decrease close to 20 K/min could be determined. The situation changes when aging is performed at temperatures ≥ 500 °C, Fig. 5b. In this case, martensitic transformations were observed for all different aging times and temperatures. The data in Fig. 5b show that the most severe change in transformation temperatures occurs during aging at 500 °C. After ≈ 20 min at 500 °C, the M_S temperature dropped from 180 to 120 °C. For all other heat treatment temperatures considered in Fig. 5b, small minima were observed after short annealing times. Afterwards, constant M_S levels were reached. It is reasonable to assume that these apparent minima represent artifacts because it is likely that the samples could not reach the target aging temperatures within short annealing times. Therefore, microstructural evolution processes governed by transient thermodynamic driving forces are responsible for a temporary drop of M_S . After passing the apparent $M_S(t)$ minimum, aging at 600 °C results in a constant M_S temperature close to 160 °C after 20 min thermal exposure. In case of aging at 800 °C, M_S values slightly higher than the initial M_S temperature could be maintained throughout the complete aging procedure, after passing the minimum mentioned above, Fig. 5b.

Figure 6 presents a different visualization of the data previously shown in Fig. 5. The M_S data in Fig. 6 are plotted as a function of the aging temperature. The various

data sets correspond to different aging durations. The dashed red horizontal line indicates the original M_S temperature of the $\text{Ti}_{70}\text{Ta}_{30}$ HTSMA prior to aging. The black vertical dashed line represents the β transus temperature which was derived from the Ti–Ta phase diagram, Fig. 1 [36]. The results presented in Fig. 6 suggest that, in general, aging at temperatures below 800 °C affects martensitic transformation behavior in $\text{Ti}_{70}\text{Ta}_{30}$. The most significant change of M_S occurs during aging at temperatures close to 400 °C. The fact that a decrease of M_S can be observed after annealing at 600 °C, which is slightly higher than the β transus temperature derived from the phase diagram in Fig. 1, suggests that the latter is inaccurate.

Evolution of Microstructures During Aging

In the present work, an effort was made to identify the microstructural processes which govern functional degradation. We show that specific types of microstructures

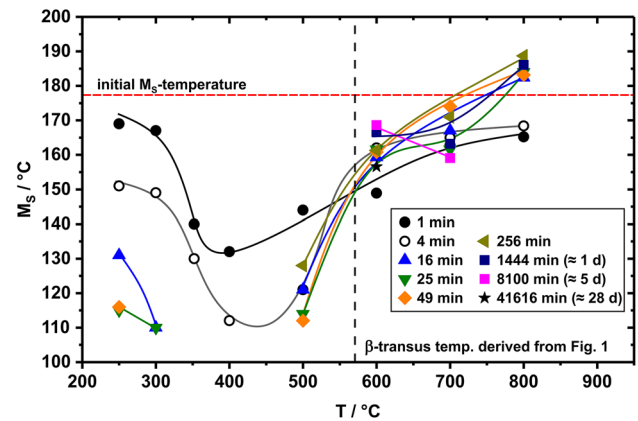


Fig. 6 Dependence of M_S on aging conditions. M_S data are plotted as a function of aging temperature. The various data sets correspond to different aging durations (Color figure online)

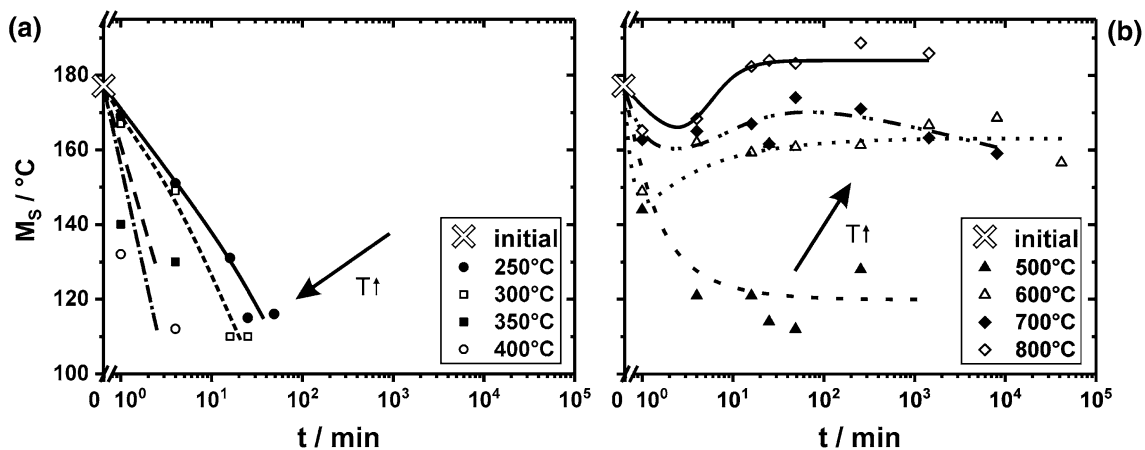


Fig. 5 Effect of aging conditions on M_S . Aging temperature range **a** 250–400 °C, and **b** 500–800 °C

evolve when the material is subjected to annealing in different temperature regimes.

Annealing at low temperatures results in the formation of ω phase. In Fig. 7, the results of TEM investigations on $\text{Ti}_{70}\text{Ta}_{30}$ after aging at 300 °C for 30 min are presented. Figure 7a shows a TEM bright-field image of the microstructure. In the bright-field image, a circle labels the region from which selected area diffraction (SAD) analysis was obtained, presented in Fig. 7b. Figure 7b shows a diffraction pattern of the [0-1-1]-zone direction of the bcc phase. Beside the fundamental reflections of the bcc phase, reflections at $1/3 \{211\}$ positions are visible indicating the presence of variants of the ω phase, explained by the schematic illustration presented in Fig. 7c. As shown, one set of $1/3 \{211\}$ -type reflections belongs to one variant of

the ω phase. With one $1/3 \{211\}$ reflection labeled with a white circle in Fig. 7b, a TEM dark-field image was obtained, Fig. 7d. The dark-field image reveals precipitation of the ω phase with particle sizes of a few nm and a high number density. No traces of martensitic α'' phase can be observed in the TEM sample.

Figure 8 shows the results of the TEM investigations on $\text{Ti}_{70}\text{Ta}_{30}$ after an extended aging heat treatment conducted at 400 °C for 41,616 min, which corresponds to ≈ 29 days. In the scanning transmission electron microscopy (STEM) HAADF image presented in Fig. 8a, which was obtained with a small camera length of 50 mm, thus mass density contrast is dominating, regions with dark and bright contrast appear. Figure 8b shows a selected area electron diffraction pattern of the $[101]_{\text{bcc}}$ zone direction of

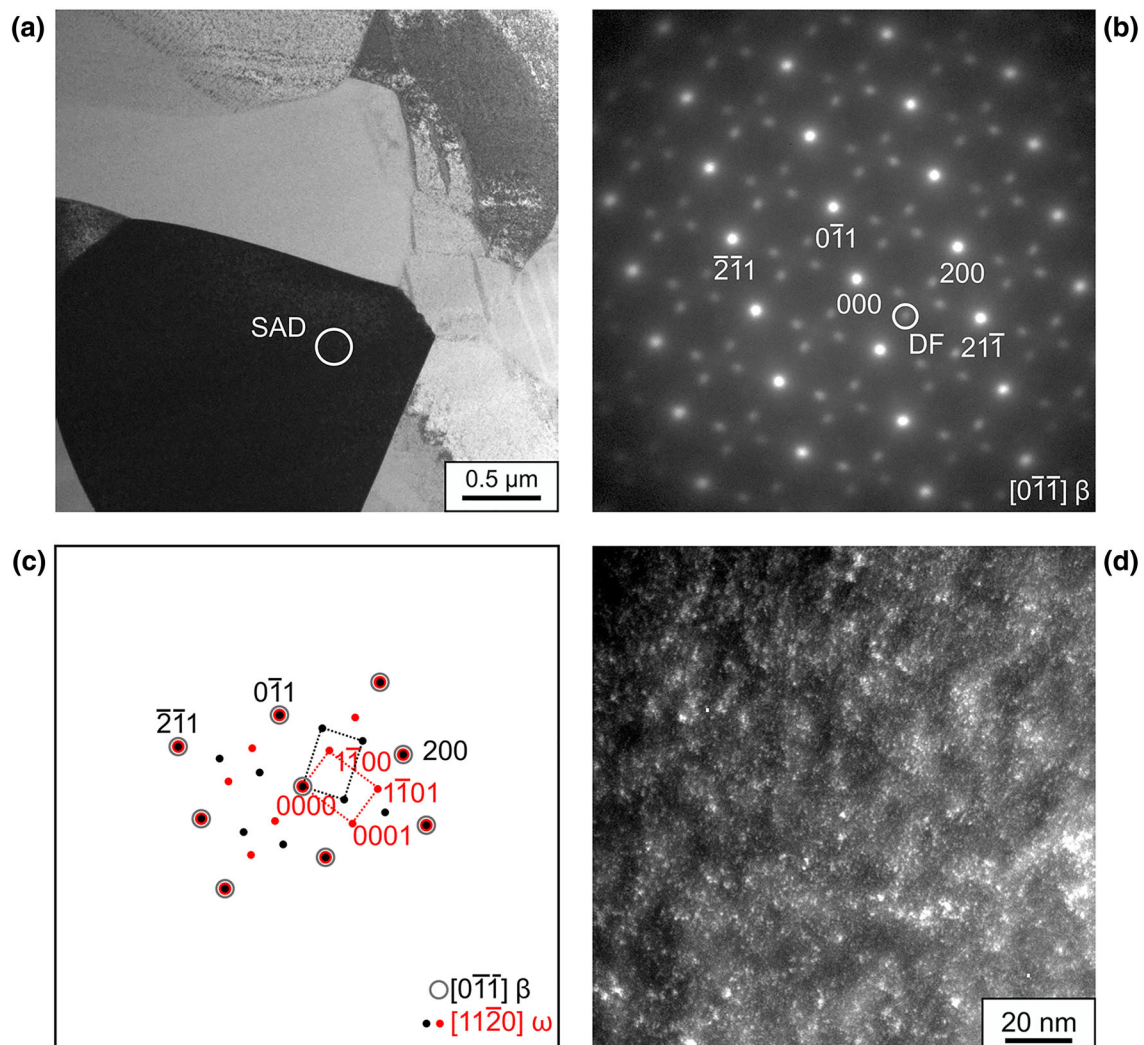


Fig. 7 Presence of ω phase in $\text{Ti}_{70}\text{Ta}_{30}$ after aging at 300 °C for 30 min. **a** TEM bright-field image, **b** selected area diffraction pattern of the circular region marked in **(a)** with “SAD”, Miller indices refer to the β phase, **c** schematic interpretation of diffraction results

involving β phase and two ω phase variants. **d** TEM dark-field image obtained from the $1/3 \{211\}$ -type reflection labeled with a white circle in **(b)** (Color figure online)

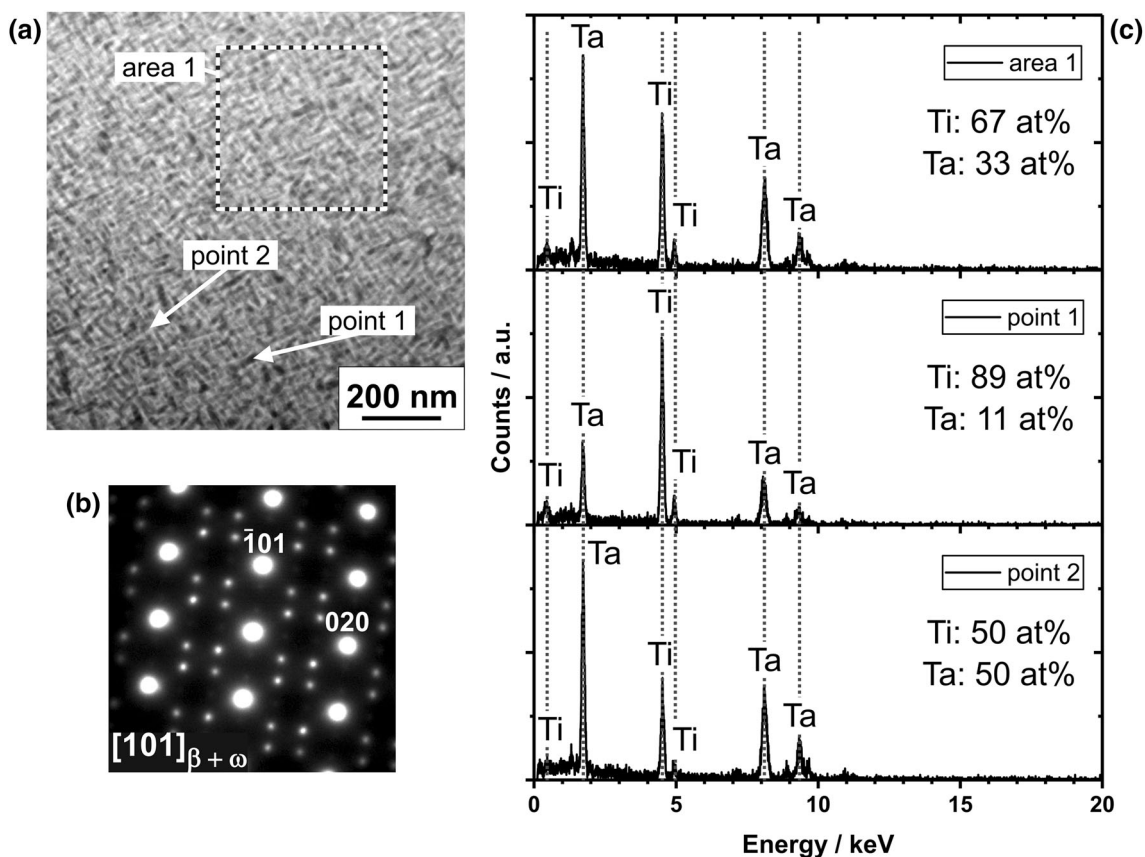


Fig. 8 TEM analysis of the microstructure resulting from aging at 400 °C for a long duration of 41,616 min (close to 29 days). **a** HAADF STEM image, **b** SAD pattern, **c** EDX analysis of sample regions indicated in **(a)**

the β phase. In addition to the fundamental reflections of the bcc phase, the $1/3 \{211\}$ reflections reveal the presence of ω phase. Chemical analysis with EDX was performed on a position with dark contrast and on a position with bright contrast labeled with “point 1” and “point 2” in Fig. 8a, respectively. The EDX analysis presented in Fig. 8c shows a Ti content of about 90 at% for the ω phase and a Ti content of 50 at% for the β phase, while the average chemical composition of the area labeled with a dashed square in Fig. 8a is with 67 at% close to the nominal alloy composition of 70 at%. These findings suggest that the formation of a Ti-rich ω phase during aging enriches the bcc matrix in Ta.

Figure 9 provides synchrotron diffractograms obtained from different aged material states. In Fig. 9, the * symbols indicate positions of diffraction peaks related to β phase. The blue-dashed lines indicate peak positions which are exclusively related to ω phase. The black-dashed lines show positions of isolated α phase peaks, and peaks marked with a + symbol document the presence of α'' martensite. Figure 9 allows to identify the following trends. In contrast to the initial material state (Fig. 2c), aging results in the formation of microstructures which are characterized by

the presence of the high-temperature β phase and precipitates. Only in case of low-temperature aging at 250 °C for 1444 min, a small volume fraction of α'' martensite could be detected. This material state also contains ω phase, which can be concluded from characteristic superlattice peaks with weak intensities. However, with increasing aging duration, the presence of ω phase becomes more evident. As we move from the sample aged at 250 °C for 1444 min to a sample aged for a longer time of 41,616 min, especially the $(302)_{\omega}$ peak appears more pronounced. We note that—generally—even relatively high volume fractions of ω phase result in XRD/SD diffraction events with only weak intensities. Nevertheless, diffraction peaks related to ω phase appear clearer when the aging temperature is increased to 300 and 400 °C. In this case, several specific ω phase peaks can be identified. Furthermore, the diffractograms from these material states also suggest that small amounts of α phase are present. Table 1 provides information on lattice parameters of the different phases. The data in Table 1 were obtained by Le Bail refinement of synchrotron X-ray diffractograms from the material states resulting from different aging treatments. We note that our lattice parameters for ω phase are

Fig. 9 Synchrotron diffraction data documenting the presence of α , α'' , β , and ω phase after different aging treatments (Color figure online)

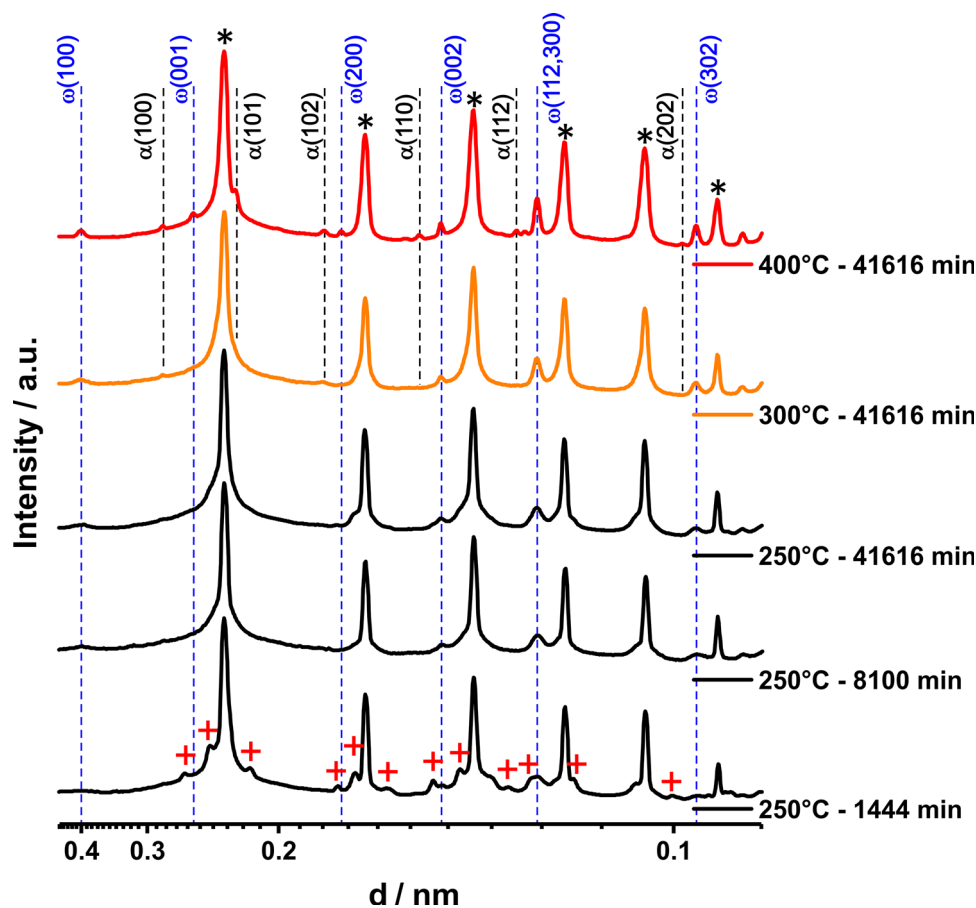


Table 1 Lattice constants of different phases in material states resulting from aging at 300, 400, and 600 °C for 41,616 min

T (°C)	Phase	a (10 ⁻¹ nm)	b (10 ⁻¹ nm)	c (10 ⁻¹ nm)
300	α	2.965	–	4.698
	β	3.2814	–	–
	ω	4.654	–	2.833
400	α	2.944	–	4.727
	β	3.2839	–	–
	ω	4.631	–	2.835
600	α	2.9514	–	4.703
	α''	3.222	4.758	4.653
	β	3.2890	–	–

similar to values reported recently by Lai et al. [57] for Ti-Nb alloys.

Figure 10 presents examples of SEM micrographs of material states which result from aging at 400 °C. Figure 10a shows a SEM micrograph (obtained in BSE mode) where some martensite twins and small precipitates located on prior austenite grain boundary regions can be observed. The white-dashed rectangle in Fig. 10a indicates a region with grain boundary particles which is presented in Fig. 10b at higher

magnification. Figure 10b (BSE contrast) shows that these particles have sizes less than 100 nm. The dark and bright contrasts suggest that the two types of particles have different Ti/Ta ratios. This is in line with previous TEM EDX results reported in [45, 49]. We note that the dark phase could be identified by TEM analysis as α Ti (hex) with a Ti concentration close to 90 at%, and the bright phase as a Ta-rich β phase (TEM results not shown here). Figure 10c and d document that the size of these particles increases with aging time. After a longer aging time of 41,616 min, the dark Ti-rich particles are often characterized by elongated shapes, Fig. 10c and d. They are still mainly located in grain boundary regions as shown in the high-magnification SEM micrograph presented in Fig. 10d. The material resulting from long-term aging treatments at 400 °C allows to identify one additional feature. A close look at the apparent matrix of the microstructure shown in Fig. 10d and e reveals the presence of a high density of fine nano-sized particles which provide different contrasts. These particles represent ω phase and Ta-rich β , which had been previously identified by TEM, Fig. 8.

We now move to the material states which result from aging at a higher temperature of 600 °C, Fig. 11. Figure 11 shows SEM micrographs obtained after aging at 600 °C for 49 min, Fig. 11a and b, and for 41,616 min, Fig. 11c and

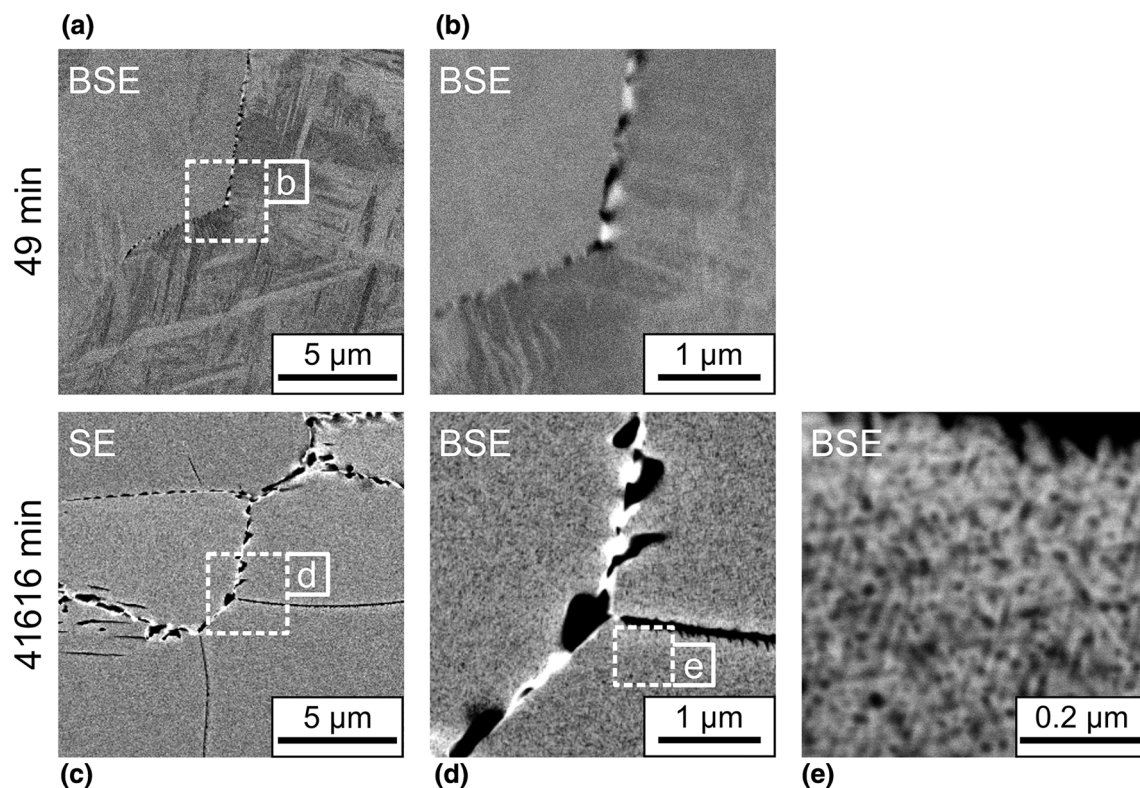


Fig. 10 Microstructures of $\text{Ti}_{70}\text{Ta}_{30}$ after aging at $400\text{ }^{\circ}\text{C}$. The SEM micrographs were obtained after aging times of (a, b) 49 min and (c, d, and e) 41,616 min (corresponding to ≈ 29 days). The dashed

rectangular regions in (a, c, and d) indicate microstructural parts presented in (b, d, and e) at higher magnification

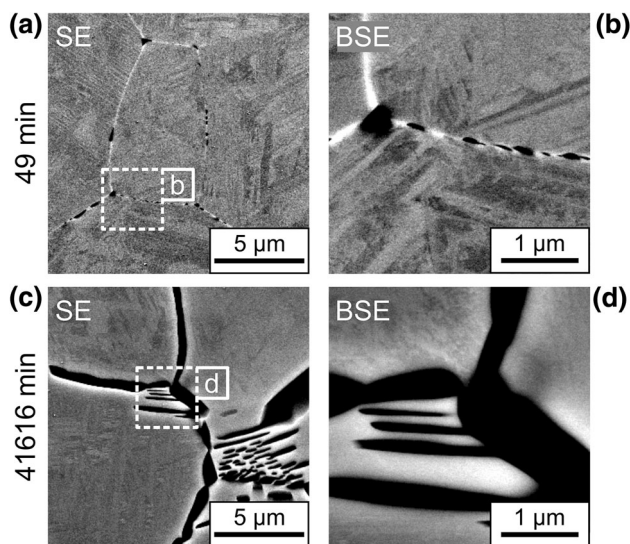


Fig. 11 Microstructures of $\text{Ti}_{70}\text{Ta}_{30}$ after aging at $600\text{ }^{\circ}\text{C}$. The SEM micrographs were obtained after aging times of (a and b) 49 min and (c and d) 41,616 min (corresponding to ≈ 29 days). The dashed squares in (a and c) indicate microstructural regions presented in (b and d) at higher magnification

d. The micrographs presented in Fig. 11b and d show regions at high magnification, which were marked in the overview images, Fig. 11a and c, by dashed rectangles.

The SEM results suggest that Ti-rich phases (dark contrast) form during aging. TEM analysis (data not shown here) reveals that these phases represent α Ti with Ti concentrations close to 94 at%. This is in line with SD results, Fig. 9. Similar to what was presented for material states subjected to aging at a lower temperature of $400\text{ }^{\circ}\text{C}$, Fig. 10, these phases mainly form in grain boundary regions. Finally, we note that the SD and TEM analyses of samples aged at 500 and $600\text{ }^{\circ}\text{C}$ (results not shown here) did not provide any evidence for the presence of ω phase. We therefore conclude, that ω phase is not stable in this temperature range. Aging appears to be solely associated with the formation of α phase on β grain boundaries. After aging in this temperature range, the remaining material volume consists of the β phase which during quenching transforms into α'' martensite. No other phases were observed in this material state.

Figure 12 presents SEM EDX data from α Ti particles which are located in grain boundary regions. These particles are shown in the two small insets of Fig. 12. The corresponding material states have been previously subjected to aging at $600\text{ }^{\circ}\text{C}$ (red curve) and at $700\text{ }^{\circ}\text{C}$ (blue curve), respectively, for 29 days. For reference, Fig. 12 also contains EDX data from high-purity α titanium, i.e., the raw material used for Ti–Ta arc melting. The

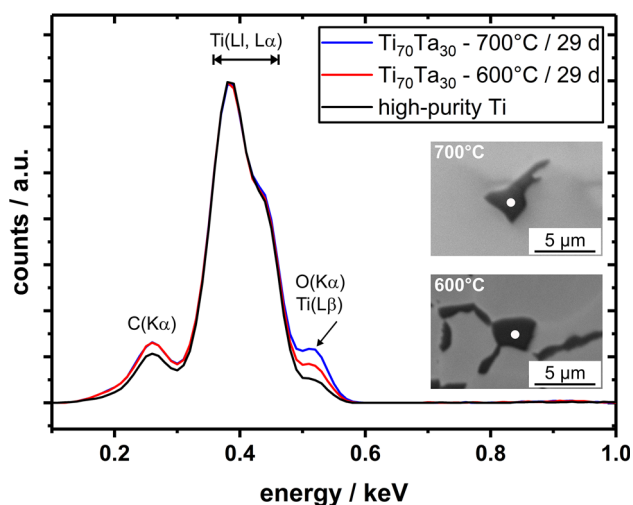


Fig. 12 SEM EDX data documenting the presence of oxygen in grain boundary α Ti particles in aged material states. The black curve originates from high-purity Ti which represents an oxygen-free reference. For details, see text (Color figure online)

backgrounds of all EDX curves have been subtracted, and all data have been normalized such that the Ti L α and L β X-ray peaks exactly coincide. Figure 12 shows one striking observation. The α Ti phases in all three materials are characterized by slightly different compositions in terms of oxygen. This can be seen at an energy close to 500 eV, where Ti L β and O K α intensities overlap. In the case of pure Ti (reference, black line), the small peak at 500 eV exclusively corresponds to Ti L β . However, in the case of the aged material states, the corresponding EDX peak intensity is significantly higher (see arrow). This finding indicates that the small grain boundary α Ti particles must contain small amounts of oxygen. The presence of O in solid solution results in a higher peak intensity as compared to the O-free reference material state. Therefore, our results suggest that oxygen plays a role for the formation of α Ti particles in grain boundary regions. In passing, we note that material state aged at 700 °C was characterized by a low particle-density of the above-mentioned α particles, and—furthermore—this material actually had a slightly increased O concentration (as mentioned in the experimental details section).

Discussion

Phase Transformation Behavior

The present study shows that the functional and microstructural stability of Ti₇₀Ta₃₀ HTSMAs could be considered as relatively poor. Exposing metastable β -Ti-Ta to elevated temperatures allows the alloy system to

approach its thermodynamic equilibrium, as defined by the phase diagram in Fig. 1. The corresponding microstructural changes occur on the time scale of minutes, hours, and days. Depending on aging conditions, these changes lead to a shift in transformation temperatures, or to a complete suppression of the martensitic transformation, Figs. 4, 5, and 6.

The microstructural results, Figs. 7, 8, 9, 10, 11, and 12, allow to identify the underlying mechanisms for the observed changes in $\beta \leftrightarrow \alpha''$ transformation behavior. Aging at lower temperatures such as 250–400 °C results in a high density of nm-sized ω phase particles, Figs. 7 and 8. It has been suggested that the formation of this type of microstructure leads to a Ta enrichment in the β matrix, and thus to a decrease in transformation temperatures [41]. While a direct evidence for this proposed mechanism was missing so far, the EDX data presented in Fig. 8 clearly provide an experimental proof for the formation of a Ti-rich ω phase and a simultaneous Ta enrichment of the β phase. However, our results suggest that also further aspects need to be considered. The results presented in Fig. 4a and b show that the DSC peak of the martensitic transformation on cooling, Fig. 4a, is strongly affected by aging than the peak related to the reverse transformation on heating, Fig. 4b. If only chemical effects were taken into account, one would expect that both transformation events decreased in almost the same way [41, 43, 44]. However, Fig. 4a and b show that that is not the case. Therefore, as a new aspect, we suggest that the high density of small ω phase particles, Fig. 7, additionally affects the formation of α'' martensite by impeding nucleation events. These ω phase particles suppress the formation of self-accommodating martensite twin structures by providing stresses and/or geometrical constraints. Therefore, the nucleation of martensite is associated with higher elastic strain energies such that a higher degree of undercooling is required to overcome the nucleation barrier [9]. In summary, the DSC and TEM results, Figs. 4a, b, 7, and 8, can be interpreted such that ω phase affects the formation of α'' martensite by altering both matrix chemistry and nucleation conditions.

The scenario suggested above may also rationalize the effects of aging at higher temperatures, Fig. 4c–f and Fig. 5b. In case of aging at 600 °C, where Ti-rich α phase forms, Fig. 11, it is reasonable to assume that the changes in $\beta \leftrightarrow \alpha''$ transformation behavior are dominated by pure compositional effects. Geometrical constraints appear to be less important since α phase particle densities are relatively low and the α phase is much coarser than ω phase, Fig. 11. The formation of Ti-rich α Ti results in a small increase of the Ta concentration in the matrix. This rationalizes the slight decrease of both M_s and latent heat, as documented in Fig. 4e and f.

We finally note that aging at 800 °C resulted in a slight increase of the M_S temperature, Figs. 5 and 6. This increase is small; however, it cannot be neglected. At present, the underlying mechanisms are not clear. It seems unlikely that chemical effects play a role. Maybe, a long-term aging treatment at 800 °C establishes a microstructure where the formation of martensite is easier than in the initial material state. Further work is required to rationalize this finding.

Extending Functional Fatigue Life

One may feel that the limited functional/microstructural stability of Ti–Ta HTSMAs can impede the use of this material in engineering applications. In fact, it is documented in literature that the microstructural evolution processes described in the present work govern functional fatigue during high-temperature actuation cycling, e.g., [47–49]. However, several attempts were reported which successfully improve fatigue life. First, Krooß et al. [46, 47] have demonstrated positive effects of a “reset heat treatment.” Intermediate heat treatments at a sufficiently high temperature resolve precipitates which have previously formed during actuation cycles, and it re-establishes (nearly) the original microstructure. This type of fatigue life improvement can be exploited for a large number of times, if required [46, 47]. On the long run, however, additional processes, such as intergranular cracking [47] become important for limiting service life.

Second, the data presented in Figs. 5 and 6 suggest that the fastest degradation of the material occurs during thermal exposure to a temperature range close to 400 °C. In case of the Ti₇₀Ta₃₀ HTSMA considered in the present work, this means that it is of utmost importance in an application to reduce the exposure to corresponding temperatures to a minimum possible duration. This can be achieved, for example, by applying high heating and cooling rates in actuation cycles.

Third, the microstructural and functional stability of Ti–Ta HTSMAs can be improved by modification of the alloy composition. Buenconsejo et al. [40] have investigated the effects of ternary alloy additions to Ti–Ta HTSMAs. They observed that adding Al and Sn to binary Ti–Ta improves the stability of the material. As a drawback, the addition of these elements results in an undesired shift of transformation temperatures to lower values. However, it has recently been demonstrated by A. Ferrari et al. [44] that additions of Al to binary Ti–Ta not necessarily result in such a decrease. In fact, the authors [44] show that Al additions decrease the martensite start temperature *only* for Ti–Ta HTSMAs with high Ta concentrations exceeding ≈ 16 at%. Surprisingly, alloying Al to Ti-lean Ti–Ta HTSMAs results in an increase of M_S !

Fourth, Ta-lean Ti–Ta HTSMAs may represent a promising candidate material. Most importantly, they are characterized by relatively high transformation temperatures [43, 49, 67]. Preliminary results suggest that the maximum temperatures in actuation cycles for these alloys can easily exceed the ω phase stability range, such that this detrimental phase dissolves. Recently, we have presented an actuator test setup at the HTSMAs 2018 conference, where Ti₇₅Ta₂₅ spring actuators prepared from thin wires were able to provide at least 200 actuation cycles, without any intermediate reset heat treatments.

A Time Temperature Transformation Plot for Ti₇₀Ta₃₀

The results of the present study allow to discuss microstructural changes during aging of Ti₇₀Ta₃₀ and related kinetics through an isothermal time temperature transformation (TTT) diagram. Figure 13 presents a simplified TTT plot which reflects the main microstructural evolution processes. Figure 13 is derived from the systematic evaluation of a large number of samples, Fig. 3, which allow to retrieve information on martensitic transformations, Figs. 4, 5, and 6, and on different types of microstructures as exemplarily presented in Figs. 7, 8, 9, 10, 11, and 12. The TTT plot presented in Fig. 13 reassembles specific trends which have been reported in comparable studies on other Ti-based alloy systems, e.g., [68–73]. The red line in Fig. 13 indicates the region where the formation of ω phase was detected, and the blue line the region where α phase forms. The dashed gray line represents the limit for the formation of α'' martensite. Material states located on the right of this line do not show

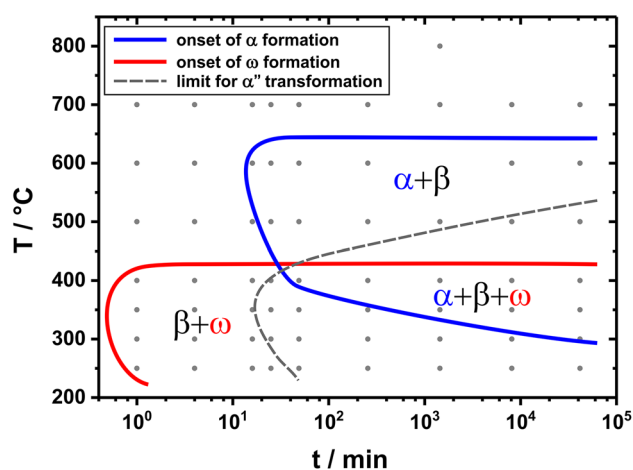


Fig. 13 Time temperature transformation diagram derived from the results of the present study. Material states on the right of the martensite transformation limit (gray line) do not show the formation of α'' martensite during cooling to room temperature (Color figure online)

a martensitic phase transformation within the experimental conditions of the present study. Figure 13 shows that the formation of ω phase is relatively fast, as it can be immediately observed after shortest annealing times. This is in line with literature data [74] where a relatively low apparent thermal activation energy of 85 kJ/mole could be determined for this process in a Ti-Mo-Nb-Al alloy. The formation of ω phase can be observed up to a temperature of at least 400 °C, Figs. 8 and 9. At temperatures > 500 °C, the precipitation of α Ti is the only dominating microstructural evolution process.

A closer look at the TTT diagram, Fig. 13, reveals the existence of a three-phase region for long aging times. This region is characterized by microstructures consisting of α Ti in grain boundary regions and β and ω in the remaining volume, Figs. 9, 10, and 11. One might worry that this finding violates the Gibb's phase rule since no more than two phases would be simultaneously allowed in a binary alloy such as Ti-Ta. However, two aspects need to be considered to rationalize this finding. First, the corresponding material states do not necessarily represent microstructural equilibria. Second, the EDX data presented in Fig. 12 suggest that oxygen as a third element is involved in the formation of grain boundary α Ti. In general, oxygen is known as a strong α stabilizer [34, 75], and therefore, it is reasonable to assume that the small amounts of oxygen, Fig. 12, play a role in phase formation processes. However, our results do not allow to identify the reasons why the corresponding regions are characterized by increased oxygen levels. In principle, the formation of these zones could be related to segregation processes or to diffusive fluxes of oxygen along grain boundaries, representing an unavoidable side-effect of long-term aging experiments, where it is impossible to fully avoid oxidation. Further work is required to clarify this.

We finally note that the TTT plot presented in Fig. 13 has a simplified character. The precision concerning the onset boundaries of the different precipitation reactions is restricted by the accuracy of the applied characterization techniques and by the analytical effort (which had to be kept in an appropriate frame). The TTT plot also does not reflect the possible formation of unusual phases such as α' martensite [76], two β phases with different compositions [77, 78], and σ phase [79], which has been suggested in other studies [76–79]. Further work is required to verify whether these phases can form in $\text{Ti}_{70}\text{Ta}_{30}$.

Summary and Conclusions

In the present study, we investigate how isothermal aging affects the martensitic transformation behavior and microstructures in $\text{Ti}_{70}\text{Ta}_{30}$ high-temperature shape-

memory alloys. We combine differential scanning calorimetry (DSC) and various advanced microstructural characterization techniques such as scanning electron microscopy (SEM), transmission electron microscopy (TEM), conventional X-ray, and synchrotron diffraction (XRD and SD). The following key findings can be reported:

- (1) In general, isothermal aging of $\text{Ti}_{70}\text{Ta}_{30}$ significantly affects the martensitic transformation. Annealing at lower temperatures, e.g., 250–400 °C, results in a decrease of M_S . Furthermore, the formation of martensite is fully suppressed after a few minutes of aging. We identify a critical temperature window which should be avoided during thermal exposure of $\text{Ti}_{70}\text{Ta}_{30}$ in applications.
- (2) We discuss possible mechanisms how different microstructural evolution processes affect the martensitic and reverse transformation. Precipitation of α and ω phases affect the $\beta \leftrightarrow \alpha'$ transformation by changing the composition of the β matrix. In case of ω phase formation, the high density of nano-size precipitates additionally seems to impede the nucleation of martensite. Therefore, a higher degree of undercooling is required to overcome the nucleation barrier.
- (3) An isothermal time temperature transformation (TTT) diagram for $\text{Ti}_{70}\text{Ta}_{30}$ was established, which allows to rationalize the formation of different types of microstructures during aging. Aging at lower temperatures, e.g., 250–400 °C, results in the formation of ω phase. The exposure of $\text{Ti}_{70}\text{Ta}_{30}$ to temperatures between 500 and 600 °C results in the formation of material states consisting of β and α titanium. The fact that this process could be observed at temperatures exceeding the apparent β transus temperature reported in literature for $\text{Ti}_{70}\text{Ta}_{30}$ indicates that the presently available Ti-Ta phase diagram is not fully accurate. The results of the present study suggest that oxygen in grain boundary regions promotes the localized formation of α Ti particles. Further work is required to rationalize this observation.
- (4) We provide a direct evidence that ω phase in $\text{Ti}_{70}\text{Ta}_{30}$ has a Ti-rich composition. We also report crystallographic data for α , α' , β , and ω phase after long-term aging treatments.
- (5) The experimental findings of the present work indicate that $\text{Ti}_{70}\text{Ta}_{30}$ HTSMAs significantly suffer from a microstructural instability. Nevertheless, Ti-Ta still represents an attractive candidate material for high-temperature shape-memory alloys. In the present work, we discuss several options which allow to slow down microstructural and functional degradation.

Acknowledgements The authors acknowledge financial support from Deutsche Forschungsgemeinschaft (DFG) through Projects TP1 (FR2675/3-2), TP2 (SO505/2-2 and EG101/22-2), and TP3 (SCHM930/13-2) in the framework of the research group FOR 1766 “Hochtemperatur-Formgedächtnislegierungen.” We acknowledge DESY (Hamburg, Germany), a member of the Helmholtz Association HGF, for the provision of experimental facilities. Parts of this research were carried out at PETRA III and we would like to thank Jozef Bednarcik for assistance in using photon beamline P02.1 and the support laboratory.

References

- Funakubo H (1987) Shape memory alloys. Gordon and Breach, New York
- Wayman CM, Deurig TW (1990) An introduction to martensite and shape memory. In: Duerig TW, Melton KN, Stöckel D, Wayman CM (eds) Engineering aspects of shape memory alloys. Butterworth-Heinemann, London
- Otsuka K, Ren X (2005) Physical metallurgy of Ti–Ni-based shape memory alloys. *Prog Mater Sci* 50(5):511–678
- Miyazaki S, Otsuka K (1989) Development of shape memory alloys. *ISIJ Int* 29(5):353–377
- Mohd Jani J, Leary M, Subic A, Gibson MA (2014) A review of shape memory alloy research, applications and opportunities. *Mater Des* 56:1078–1113
- Morgan NB (2004) Medical shape memory alloy applications—the market and its products. *Mater Sci Eng, A* 378(1–2):16–23
- Duerig TW (2002) The use of superelasticity in modern medicine. *MRS Bull* 27(2):101–104
- Van Humbeeck J (1999) Non-medical applications of shape memory alloys. *Mater Sci Eng, A* 273–275:134–148
- Bhattacharya K (2004) Microstructure of martensite: why it forms and how it gives rise to the shape-memory effect. Oxford University Press, Oxford
- Borboni A, Faglia R (2018) Robust design of a shape memory actuator with slider and slot layout and passive cooling control. *Microsyst Technol* 24(3):1379–1389
- Ma J, Karaman I, Noebe RD (2010) High temperature shape memory alloys. *Int Mater Rev* 55(5):257–315
- Yuan ZS, Lin DZ, Cui Y et al (2018) Research progress on the phase transformation behavior, microstructure and property of NiTi based high temperature shape memory alloys. *Rare Met Mat Eng* 47(7):2269–2274
- Ronald N, Tiffany B, Santo P (2006) NiTi-based high-temperature shape-memory alloys. In: Soboyejo WO, Srivatsan TS (eds) Advanced structural materials. CRC Press, Boca Raton
- Firstov GS, Van Humbeeck J, Koval YN (2004) High-temperature shape memory alloys: some recent developments. *Mater Sci Eng, A* 378(1–2):2–10
- Bucsek AN, Hudish GA, Bigelow GS, Noebe RD, Stebner AP (2016) Composition, compatibility, and the functional performances of ternary NiTiX high-temperature shape memory alloys. *Shape Mem Superelast* 2(1):62–79
- Buenconsejo PJS, Ludwig A (2014) Composition–structure–function diagrams of Ti–Ni–Au thin film shape memory alloys. *ACS Comb Sci* 16(12):678–685
- Monroe JA, Karaman I, Lagoudas DC, Bigelow G, Noebe RD, Padula S II (2011) Determining recoverable and irrecoverable contributions to accumulated strain in a NiTiPd high-temperature shape memory alloy during thermomechanical cycling. *Scripta Mater* 65(2):123–126
- Kumar PK, Lagoudas DC (2010) Experimental and microstructural characterization of simultaneous creep, plasticity and phase transformation in Ti₅₀Pd₄₀Ni₁₀ high-temperature shape memory alloy. *Acta Mater* 58(5):1618–1628
- Lin B, Gall K, Maier HJ, Waldron R (2009) Structure and thermomechanical behavior of NiTiPt shape memory alloy wires. *Acta Biomater* 5(1):257–267
- Evirgen A, Pons J, Karaman I, Santamarta R, Noebe R (2018) H-phase precipitation and martensitic transformation in Ni-rich Ni–Ti–Hf and Ni–Ti–Zr High-temperature shape memory alloys. *Shape Mem Superelast* 4(1):85–92
- Santamarta R, Evirgen A, Perez-Sierra AM et al (2015) Effect of thermal treatments on Ni–Mn–Ga and Ni-rich Ni–Ti–Hf/Zr high-temperature shape memory alloys. *Shape Mem Superelast* 1(4):418–428
- Elahinia M, Moghaddam NS, Amerinatanzi A et al (2018) Additive manufacturing of NiTiHf high temperature shape memory alloy. *Scr Mater* 145:90–94
- Zhang X, Wang Q, Zhao X, Wang F, Liu QS (2018) Study of Cu–Al–Ni–Ga as high-temperature shape memory alloys. *Appl Phys A* 124(3):6
- Jiang HX, Wang CP, Xu WW et al (2017) Alloying effects of Ga on the Co–V–Si high-temperature shape memory alloys. *Mater Des* 116:300–308
- Perez-Checa A, Feuchtwanger J, Barandiaran JM, Sozinov A, Ullakko K, Chernenko VA (2018) Ni–Mn–Ga–(Co, Fe, Cu) high temperature ferromagnetic shape memory alloys: effect of Mn and Ga replacement by Cu. *Scr Mater* 154:131–133
- Cortie MB, Kealley CS, Bhatia V, Thorogood GJ, Elcombe MM, Avdeev M (2011) High temperature transformations of the Au₇–Cu₅Al₄ shape-memory alloy. *J Alloy Compd* 509(8):3502–3508
- Tan C, Cai W, Tian X (2007) Structural, electronic and elastic properties of NbRu high-temperature shape memory alloys. *Scr Mater* 56(7):625–628
- Van Humbeeck J (1997) Shape memory materials: state of the art and requirements for future applications. *J Phys IV* 7(C5):C5-3–C5-12
- Wojcik CC (2009) Properties and heat treatment of high transition temperature Ni–Ti–Hf alloys. *J Mater Eng Perform* 18(5–6):511–516
- Canadinc D, Trehern W, Ozcan H et al (2017) On the deformation response and cyclic stability of Ni₅₀Ti₃₅Hf₁₅ high temperature shape memory alloy wires. *Scr Mater* 135:92–96
- Carl M, Van Doren B, Young ML (2018) In situ synchrotron radiation X-ray diffraction study on phase and oxide growth during a high temperature cycle of a NiTi-20 at.% Zr high temperature shape memory alloy. *Shape Mem Superelast* 4(1):174–185
- Buenconsejo PJS, Kim HY, Miyazaki S (2011) Novel beta-TiTaAl alloys with excellent cold workability and a stable high-temperature shape memory effect. *Scr Mater* 64(12):1114–1117
- Zhang J, Rynko R, Frenzel J, Somsen C, Eggeler G (2014) Ingot metallurgy and microstructural characterization of Ti–Ta alloys. *Int J Mater Res* 105(2):156–167
- Lütjering G, Williams JC (2007) Titanium. Springer, Heidelberg
- Kim HY, Miyazaki S (2018) Ni-free Ti-based shape memory alloys. Butterworth-Heinemann, Oxford
- Murray JL (1981) The Ta–Ti (Tantalum–Titanium) system. *Bull Alloy Phase Diagr* 2(1):62–66
- Bagarjatskii Y, Nosova G, Tagunova T (1958) Laws of formation of metastable phase in titanium alloys. *Dokl Akad Nauk SSSR* 122(4):593–596
- Petrzhik M, Fedotov S, Kovneristyi YK, Zhebyneva N (1992) Effect of thermal cycling on the structure of quenched alloys of the Ti–Ta–Nb system. *Met Sci Heat Treat* 34(3):190–193
- Kim HY, Fukushima T, Buenconsejo PJS, Nam T-H, Miyazaki S (2011) Martensitic transformation and shape memory properties

- of Ti-Ta-Sn high temperature shape memory alloys. *Mater Sci Eng, A* 528(24):7238–7246
40. Buenconsejo PJS, Kim HY, Miyazaki S (2009) Effect of ternary alloying elements on the shape memory behavior of Ti-Ta alloys. *Acta Mater* 57(8):2509–2515
 41. Buenconsejo PJS, Kim HY, Hosoda H, Miyazaki S (2009) Shape memory behavior of Ti-Ta and its potential as a high-temperature shape memory alloy. *Acta Mater* 57(4):1068–1077
 42. Chakraborty T, Rogal J, Drautz R (2015) Martensitic transformation between competing phases in Ti-Ta alloys: a solid-state nudged elastic band study. *J Phys: Condens Matter* 27:115401
 43. Chakraborty T, Rogal J, Drautz R (2016) Unraveling the composition dependence of the martensitic transformation temperature: a first-principles study of Ti-Ta alloys. *Phys Rev B* 94(22):224104
 44. Ferrari A, Paulsen A, Frenzel J, Rogal J, Eggeler G, Drautz R (2018) Unusual composition dependence of transformation temperatures in Ti-Ta-X shape memory alloys. *Phys Rev Mater* 2(7):073609
 45. Rynko R, Marquardt A, Paulsen A, Frenzel J, Somsen C, Eggeler G (2015) Microstructural evolution in a Ti-Ta high-temperature shape memory alloy during creep. *Int J Mater Res* 106(4):331–341
 46. Niendorf T, Krooss P, Batyrina E et al (2014) On the functional degradation of binary titanium-tantalum high-temperature shape memory alloys—a new concept for fatigue life extension. *Funct Mater Lett* 7(4):1450042
 47. Niendorf T, Krooss P, Batyrina E et al (2015) Functional and structural fatigue of titanium tantalum high temperature shape memory alloys (HT SMAs). *Mater Sci Eng, A* 620:359–366
 48. Niendorf T, Krooss P, Somsen C et al (2015) Cyclic degradation of titanium-tantalum high-temperature shape memory alloys—the role of dislocation activity and chemical decomposition. *Funct Mater Lett* 8(6):1550062
 49. Maier HJ, Karsten E, Paulsen A et al (2017) Microstructural evolution and functional fatigue of a Ti-25Ta high-temperature shape memory alloy. *J Mater Res* 32(23):4287–4295
 50. Abkowitz S, Abkowitz SM, Fisher H, Allen SM (2008) The potential of titanium-tantalum alloys for implantable medical devices. *Med Device Mater Iv*:124–129
 51. Li YC, Xiong JY, Wong CS, Hodgson PD, Wen C (2009) Ti₆Ta₄Sn alloy and subsequent scaffolding for bone tissue engineering. *Tissue Eng Pt A* 15(10):3151–3159
 52. Motemani Y, Kadletz PM, Maier B, et al. (2015) Microstructure, shape memory effect and functional stability of Ti67Ta33 thin films. *Adv Eng Mater* 17(10):1425–1433
 53. Motemani Y, Buenconsejo PJS, Craciunescu C, Ludwig A (2014) High-temperature shape memory effect in Ti-Ta thin films sputter deposited at room temperature. *Adv Mater Interfaces* 1(3):140019
 54. Sikka SK, Vohra YK, Chidambaram R (1982) Omega-phase in materials. *Prog Mater Sci* 27(3–4):245–310
 55. Hickman BS (1968) Omega phase precipitation in titanium alloys. *J Met* 20(8):A121
 56. Ohmori Y, Ogo T, Nakai K, Kobayashi S (2001) Effects of ω -phase precipitation on beta \rightarrow α , α' transformations in a metastable β titanium alloy. *Mater Sci Eng, A* 312(1–2):182–188
 57. Lai MJ, Tasan CC, Zhang J, Grabowski B, Huang LF, Raabe D (2015) Origin of shear induced β to ω transition in Ti-Nb-based alloys. *Acta Mater* 92:55–63
 58. Banerjee S, Tewari R, Dey GK (2006) Omega phase transformation—morphologies and mechanisms. *Int J Mater Res* 97(7):963–977
 59. Li T, Kent D, Sha G, Dargusch MS, Cairney JM (2015) The mechanism of ω -assisted α phase formation in near β -Ti alloys. *Scr Mater* 104:75–78
 60. Prima F et al (2000) ω precipitation in a beta metastable titanium alloy, resistometric study. *Mater Trans, JIM* 41(8):1092–1097
 61. Li T, Kent D, Sha G et al (2016) New insights into the phase transformations to isothermal ω and ω -assisted α in near β -Ti alloys. *Acta Mater* 106:353–366
 62. Collings EW (1975) Magnetic studies of omega-phase precipitation and aging in titanium-vanadium alloys. *J Less Common Met* 39(1):63–90
 63. Frenzel J, George EP, Dlouhy A, Somsen C, Wagner MFX, Eggeler G (2010) Influence of Ni on martensitic phase transformations in NiTi shape memory alloys. *Acta Mater* 58(9):3444–3458
 64. Lutterotti L (2010) Total pattern fitting for the combined size-strain-stress-texture determination in thin film diffraction. *Nucl Instrum Methods B* 268(3–4):334–340
 65. Lutterotti L, Gualtieri A, Aldighetti S (1996) Rietveld refinement using Debye-Scherrer film techniques. *Eur Powder Differ* 228:29–34
 66. Dippel AC, Liermann HP, Delitz JT (2015) Beamline P02. 1 at PETRA III for high-resolution and high-energy powder diffraction. *J Synchrotron Radiat* 22(3):675–687
 67. Paulsen A (2019) Herstellung, Eigenschaften und Phastenstabilitäten von Hochtemperaturformgedächtnislegierungen auf Basis von Ti-Ta. Thesis, Ruhr-Universität Bochum, Bochum
 68. Feeney JA, Blackburn MJ (1970) Effect of microstructure on the strength, toughness, and stress-corrosion cracking susceptibility of a metastable beta titanium alloy (Ti–11.5 Mo–6Zr–4.5 Sn). *Metall Trans* 1(12):3309–3323
 69. Rhodes CG, Williams JC (1975) The precipitation of α -phase in metastable β -phase Ti alloys. *Metall Trans A* 6(11):2103–2114
 70. Williams J, Hickman B, Leslie D (1971) The effect of ternary additions on the decomposition of metastable beta-phase titanium alloys. *Metall Trans* 2(2):477–484
 71. Chen F, Xu G, Zhang X, Zhou K (2017) Isothermal kinetics of $\beta \leftrightarrow \alpha$ transformation in Ti-55531 alloy influenced by phase composition and microstructure. *Mater Des* 130:302–316
 72. Bönisch M, Panigrahi A, Calin M et al (2017) Thermal stability and latent heat of Nb-rich martensitic Ti-Nb alloys. *J Alloy Compd* 697:300–309
 73. Aeby-Gautier E, Bruneseaux F, Da Costa Teixeira J, Appolaire B, Geandier G, Denis S (2007) Microstructural formation in Ti alloys: in-situ characterization of phase transformation kinetics. *JOM* 59(1):54–58
 74. Hui Q, Xue XY, Kou HC, Lai MJ, Tang B, Li JS (2013) Kinetics of the omega phase transformation of Ti-7333 titanium alloy during continuous heating. *J Mater Sci* 48(5):1966–1972
 75. Wahlbeck PG, Gilles PW (1966) Reinvestigation of the phase diagram for the system titanium-oxygen. *J Am Ceram Soc* 49(4):180–183
 76. Ikeda M, Komatsu S-Y, Nakamura Y (2002) The effect of Ta content on phase constitution and aging behavior of Ti-Ta binary alloys. *Mater Trans* 43(12):2984–2990
 77. Ikeda M, Komatsu S-Y, Nakamura Y (2004) Effects of Sn and Zr additions on phase constitution and aging behavior of Ti-50 mass% Ta alloys quenched from β single phase region. *Mater Trans* 45(4):1106–1112
 78. Barzilai S, Toher C, Curtarolo S, Levy O (2016) Evaluation of the tantalum-titanium phase diagram from ab-initio calculations. *Acta Mater* 120:255–263
 79. Kadletz PM, Motemani Y, Iannotta J et al (2018) Crystallographic structure analysis of a Ti-Ta thin film materials library fabricated by combinatorial magnetron sputtering. *ACS Comb Sci* 20(3):137–150